Effects of electric field and interlayer coupling on Schottky barrier of germanene/MoSSe vertical heterojunction

Jun Yuan,[1] Fanfan Wang,[1] Zhufeng Zhang,[1] Baoan Song,[2] Shubin Yan,[3]
Ming-Hui Shang,[4] Chaohui Tong,[1,*] and Jun Zhou[1,†]

[1]*School of Physical Science and Technology, Ningbo University, Ningbo 315211, Zhejiang, People's Republic of China*
[2]*Faculty of Electrical Engineering and Computer Science, Ningbo University, Ningbo 315211, People's Republic of China*
[3]*School of Electrical Engineering, Zhejiang University of Water Resources and Electric Power, Hangzhou 310018, People's Republic of China*
[4]*Institute of Micro/Nano Materials and Devices, Ningbo University of Technology, Ningbo City 315211, People's Republic of China*

(Received 11 November 2022; revised 2 August 2023; accepted 25 August 2023; published 5 September 2023)

Among the many two-dimensional materials, germanene and Janus MoSSe have received considerable attention due to their novel electrical and optical properties. We anticipate that the heterojunction formed by germanene and MoSSe will exhibit exceptional properties and immense potential for applications in optoelectronic devices. Here, germanene/MoSSe vertical heterojunctions (VHJs) have been constructed by stacking the twisted bilayers, and their electronic properties, structural stability, and interface characteristics are calculated by applying the density functional theory. Meanwhile, the *ab initio* molecular dynamics simulation shows that the germanene/MoSSe VHJs are thermodynamically stable, and the germanene/SeMoS (Ge/SeMoS) VHJ is more energetically stable than germanene/SMoSe (Ge/SMoSe) VHJ. The Schottky contact is formed in the germanene/MoSSe heterojunctions. In particular, the Schottky barrier of Ge/SeMoS VHJ can be modulated by the electric field, resulting in the change of Schottky contact from p-type to n-type, even to Ohmic contact. However, the change in interlayer distance also can lead to variation of the Schottky barrier, but the contact type is unchanged. In addition, the Ge/SeMoS VHJ exhibits an excellent light absorption performance. Therefore, the Ge/SeMoS VHJ is a potential material for the design and fabrication of optoelectronic devices.

DOI: 10.1103/PhysRevB.108.125404

I. INTRODUCTION

Graphene is a material that is tightly packed with carbon atoms connected by sp^2 hybridization into a single two-dimensional (2D) honeycomb lattice structure that has excellent optical, electrical, and mechanical properties [1–5]. Graphene is considered a competitive alternative to silicon and displays important application prospects in materials science, energy, biomedicine, and so forth [6–8]. Inspired by the great prospects of graphene, a large number of 2D materials have been explored, such as transition metal dichalcogenides (TMDCs) [9], 2D transition metal carbides and carbonitrides (MXene) [10], monoelemental 2D semiconductors (silicene, phosphorene, germanene, etc.) [11], and hexagonal boron nitride (h-BN) [12]. Especially, low buckled (originally from the sp^2–sp^3 hybridization) germanene, like graphene, was theoretically predicted to have a Dirac cone band structure which gives rise to high carrier mobility [13]. However, comparing with graphene, the band gap of germanene is more easily opened due to its low buckled structure. [14] And then, germanene was successfully synthesized by chemical vapor deposition (CVD) on the gold (111) surface [15]. In addition, nonsymmetric Janus 2DMs have been recently proposed and prepared by CVD [16,17]. As typical Janus 2D material, the band gap and carrier mobility of MoSSe is dependent on the layers of MoSSe [18]. Moreover, the built-in electric field is generated in the vertical direction of MoSSe because of the symmetry breaking, which promotes the separation of excitons, thereby facilitating the photocatalytic reaction [19,20]. Thus, MoSSe are also promising materials for designing and constructing nanoelectronic and optical devices [21,22].

In parallel with the effort on single 2D material, the various van der Waals (vdW) heterojunctions have been made by stacking different 2D materials on top of each other and researched over the past ten years [23]. For example, Xu *et al.* showed that graphene/MoS_2 heterojunction has high charge mobility and tunability Fermi level, due to the Dirac cone of graphene preserved in the heterojunction [24]. Deng *et al.* confirmed that the black phosphorus/MoS_2 heterojunction has high photodetection responsivity and photovoltaic energy conversion because of the high mobility and appropriate direct band gap of black phosphorus [25]. Nourbakhsh *et al.* proposed that a MoS_2/WSe_2 heterojunction-based transistor exhibits a positive-to-negative transconductance due to the tunable charge density and energy band of the heterojunction [26]. In terms of broad-band photodetection and solar energy harvesting, the germanene-based heterojunctions have been explored in various methods for their perfect properties. For

*Corresponding author: tongchaohui@nbu.edu.cn
†Corresponding author: zhoujun@nbu.edu.cn

germanene/MoS_2 heterojunction, its optical absorption shows a wider range together with a redshift absorption edge [27]. A similar situation arises in germanene/AlN heterojunction, that is, optical absorption exhibits relatively enhanced trends, in the visible range and the ultraviolet light zone [28]. In addition, various MoSSe-based heterojunctions have been investigated in recent years. For instance, Li *et al.* found that for the graphene/SMoSe heterojunction, the Schottky barrier at the heterointerface can be reduced by increasing the interlayer distance, and even changing to Ohmic contact by applying a negative electric field [29]. Zhao *et al.* demonstrated that the in-plane tensile strain induces a transition from Schottky to Ohmic behavior in MoSSe/germanene heterojunction [30,31]. Recently, it was found that the constructed MoSSe/WSSe vertical heterosjunction (VHJ) presents a type-II band alignment, which is beneficial to exciton dissociation and thus highly desirable for energy conversion [32]. All the above shows that constructing of 2D material heterojunction is a very effective way of designing new devices because the heterojunctions can modulate the optical and electronic characteristics of devices to desired performance.

In this work, in view of the electronic characteristics of germanene and MoSSe mentioned above, the heterojunction structures composed of these materials are expected to have excellent optoelectronic performances and present great application potential for designing of devices. Specifically, two twisted germanene/MoSSe VHJs, Ge/SMoSe and Ge/SeMoS VHJs, are constructed by stacking germanene and Janus 2D MoSSe monolayers, respectively. By comparing the binding energy of the two germanene/MoSSe VHJs, Ge/SeMoS VHJ was selected for further investigation due to its more stable structure. And the electronic property, interfacial characteristic, and optical performance of Ge/SeMoS VHJ was examined by means of the density functional theory (DFT). The results show that the carriers in the heterojunction have very low effective mass, resulting in their high mobilities. And it is noteworthy that there is a transformation from p-type to n-type Schottky contact and even to Ohmic contact at the contact interface under the modulation of the external electric field, while interlayer distance can regulate the Schottky barrier height (SBH) but not the contact type. Moreover, the optical properties of Ge/SeMoS VHJ are explored by calculating of the dielectric constant and absorption spectrum.

II. COMPUTATIONAL DETAILS

All numerical simulations were conducted employing first-principles calculations based on density functional theory (DFT) with the linear combination of atomic orbitals (LCAO) in the Quantum Atomistix ToolKit (ATK2021) package [33,34]. The generalized gradient approximation (GGA) exchange-correlation potential with the parametrization of Perdew-Burke-Ernzerhof (PBE) was used in the geometry optimization [35,36]. The semi-empirical corrected Grimme DFT-3 model was used to investigate the vdW interaction in the germanene/MoSSe interface [37]. Heyd-Scuseria-Ernzerhof (HSE06) hybrid functional was adopted to obtain the accurate electronic band structure [38]. The pseudopotential was set to PseudoDojo [39]. Considering the full relaxation of material structures, the average force on each atom was set to less than 0.001 eV/Å and the stress error tolerance was 0.0001 eV/$Å^3$, and the optimizer method is L-BFGS algorithm. A vacuum layer of thickness 20 Å was inserted along with the c axis direction of the heterojunction to avoid the interaction between adjacent layers. The energy convergence criterion of self-consistent process was set as 10^{-5} eV and maximum iteration steps was set to 200. By the convergence test (Fig. S1[40]) of the system, and the balance of the calculation time and the calculation accuracy, a density mesh cutoff was set to 95 Hartree, and a $19 \times 19 \times 1$ Monkhorst-Pack k-points grid was sampled in the first Brillouin zone for monolayer, and the corresponding settings were 105 Hartree and $5 \times 5 \times 1$ k-points grid for the germanene/MoSSe VHJs.

III. RESULTS AND DISCUSSION

Firstly, we studied the electronic properties of germanene and Janus MoSSe monolayers. As shown in Fig. 1(a), the germanene displays a honeycomb lattice pattern with warping structure due to the coexistence of sp^2 and sp^3 hybridizations [13,14]. The MoSSe displays a sandwich geometry structure, its upper and lower layers are respectively S(Se) and Se(S) atoms, Mo layer in the middle, as shown in Fig. 1(b). Through structural optimization, we obtained the results consistent with the previous data, i.e., the lattice constants of germanene and MoSSe are 4.037 Å and 3.25 Å, the bond lengths of Ge-Ge, Mo-S and Mo-Se are 2.44 Å, 2.42 Å and 2.55 Å, respectively [14,41,42]. In Fig. 1(c), the band structures of germanene possess a Dirac cone with zero band gap at K point, indicating a semi-metallic characteristic the same as the graphene. However, we can see from Fig. 1(d), Janus MoSSe is a semiconductor with a direct band gap of 2.03 eV, which agrees well with the reported experimental measurement [16]. It should be noted that the spin orbit coupling (SOC) is not accounted in the computation of the energy band structure of electronic state for the monolayer as no significant change [30]. In addition, the phonon spectra are shown in Fig. 1(e) and 1(f) confirm that the germanene and Janus MoSSe are dynamically stable at equilibrium state due to nonnegative phonon energy. Furthermore, to better understand the atomic contribution to the energy band of MoSSe, the projected band structure of MoSSe was calculated and shown in Fig. 2. It was found that every kind of atom has different contributions to the band at different positions. Specifically, Fig. 2(a) displays the contributions of p-orbital of sulfur for MoSSe electronic band structure. In the same way, the contributions of p-orbit of Se atom and d-orbital of Mo atom are presented in Fig. 2(b) and 2(c), respectively. It can be further seen that p-orbital of S atom and d-orbital of Mo atom are the main contributors to the valence-band edge state of MoSSe, but the contribution of S atom is very limited at the K point in the Brillouin zone. The p-orbital of Se atom and d-orbital of Mo atom is dominant for the conduction-band edge state of MoSSe, however, the contribution of Se atom is very small at the K point in the Brillouin zone. So, the main contribution of the energy band edge state of MoSSe at the K point comes from d-orbital of Mo atom because of the highly localized d orbitals at Mo atom sites, which is similar to that of MoS_2 [43,44]. From the above analysis, it can be further found that the valence band maximum (VBM) and the conduction band minimum

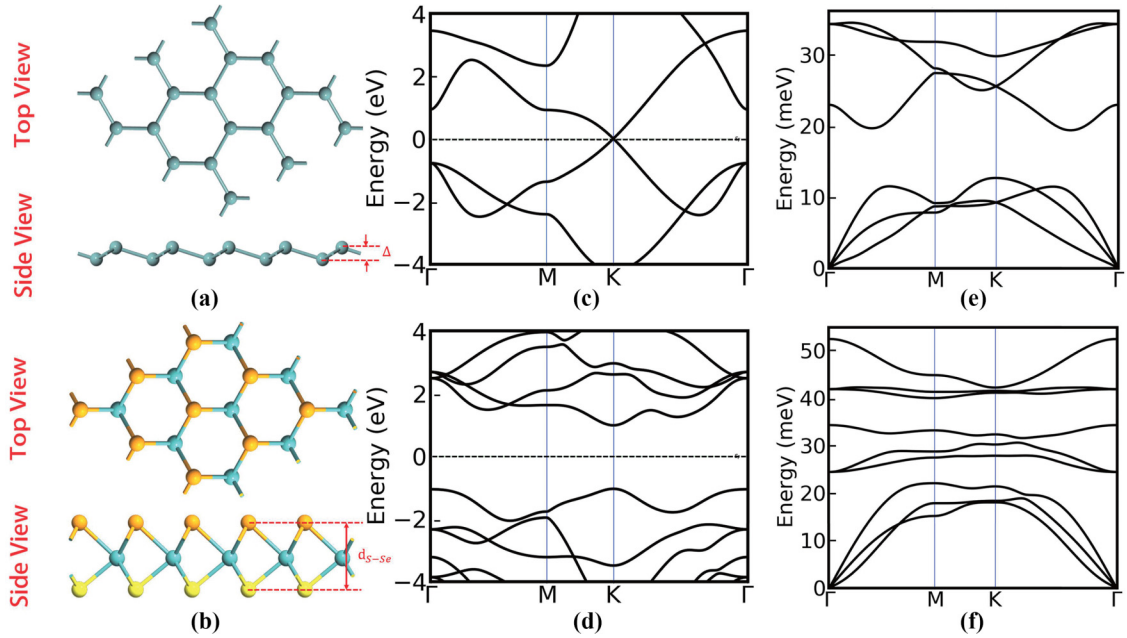

FIG. 1. Atomic structure of (a) germanene and (b) MoSSe monolayers(yellow, orange and wathet blue represent sulfur, selenium and molybdenum respectively); band structure of electronic states of (c) germanene and (d) MoSSe monolayers; phonon dispersion curves of (e) germanene and (f) Janus MoSSe monolayers.

(CBM) are distributed in the S and Se sides of the sandwich structure of MoSSe, respectively. Meanwhile, the different electro-negativity values on the two sides of MoSSe layer are due to the different atoms on its two sides. Calculation of electrostatic potential shows that there is electrostatic potential difference of ∼0.596 V between two sides of MoSSe layer, as shown in Fig. 3(a). Visually, Fig. 3(b) gives the polarized electric field generated in the MoSSe intralayer and the spatial distribution of conduction band (CB) and valence band (VB) of MoSSe, respectively. Thus, it implies that the photogenerated carriers can be rapidly separated in MoSSe under the irradiation of light, and the recombination of carriers can be also significantly reduced.

In our study, the twisted germanene/MoSSe VHJs were constructed by placing germanene on MoSSe with an interlayer angle of 46.1°. Considering different chalcogen atoms located on the opposite sides of Janus MoSSe, two heterojunctions (Ge/SMoSe and Ge/SeMoS VHJs) were assembled by the generalized lattice match (GLM) method and were separately depicted in Figs. 4(a) and 4(d) [45]. In detail, a $3 \times 3 \times 1$ supercell of germanene monolayer and $\sqrt{13} \times \sqrt{13} \times 1$ supercell of MoSSe monolayer are selected to construct the germanene/MoSSe VHJs (Fig. S2[40]). It is noted that there is an average strain of 2.14% between the germanene and MoSSe layers. However, the optoelectronic properties of TMDCs are sensitive to strain while germanene is not, so we have applied the strain to the germanene layer and the supercell lattice constant (a) of heterojunction is 11.73 Å [46,47]. After enough relaxation, the germanene and MoSSe monolayer only sffuer the strain of 1.41% and 1.87%, respectively, and the supercell lattice constant (a) is 11.94 Å. The interlayer distances (D) of the germanene and MoSSe, buckling height of germanene layer (Δ), the height of MoSSe layer ($d_{\text{S-Se}}$) are shown in Table I, respectively. To further investigate the interactions between germanene and Janus MoSSe, the electron location function (ELF) was calculated to explain bonding behaviors [48,49]. Figures 4(b) and 4(e) presents the ELF results for Ge/SeMoS and Ge/SMoSe VHJs, respectively. As

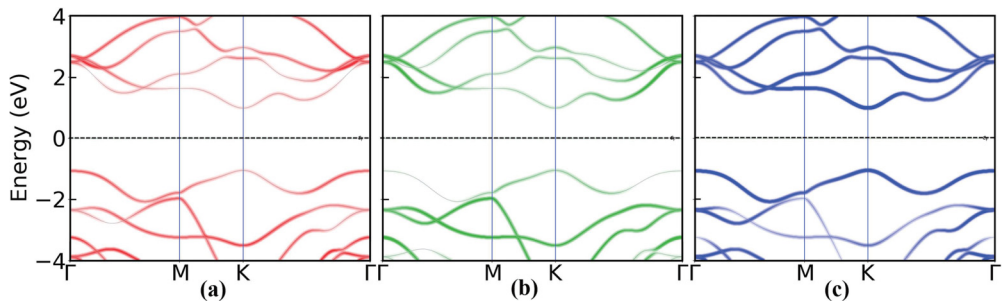

FIG. 2. Contribution of different atom orbits for energy band of MoSSe monolayer: (a) p-orbital of sulfur; (b) p-orbital of selenium; (c) d-orbital of molybdenum.

TABLE I. Interlayer distance D, buckling height of germanene layer Δ, the height of MoSSe layer $d_{\text{S-Se}}$, the supercell lattice constant of heterojunction a, binding energy E_b, band gap E_g, and difference of Schottky barrier $\Delta\Phi$.

	D(Å)	Δ(Å)	$d_{\text{S-Se}}$(Å)	a (Å)	E_b (meV/ Å^2)	E_g (meV)	$\Delta\Phi$ (eV)
Ge/SMoSe	2.99	0.72	3.21	11.73	−5.93	17.30	0.616
Ge/SeMoS	3.11	0.77	3.21	11.73	−6.23	15.78	0.266

shown in Figs. 4(b) and 4(e), the ELF value in the germanene monolayer is large and indicates the existence of covalent bonds between Ge atoms. Similarly, the ELF values in the MoSSe layer also present the covalent bonds feature between Mo and S (Mo and Se) atoms. However, the small ELF values between germanene and MoSSe monolayers demonstrate that no bonding of interlayer. In other words, there is a weak interaction between germanene and MoSSe monolayers, suggesting the constructed germanene/MoSSe VHJs are van der Waals heterojunction. Here, the ELF analyses conform with that of the vdW heterojunctions in Refs. [50–52].

In addition, the thermal stability of the constructed heterojunctions was examined by *ab initio* molecular dynamics (AIMD). As shown in Figs. 4(c) and 4(f), there is no structure distortion in two heterojunctions under heating at 300 K for 4 ps, and the change of potential energy is very small during heating period. Therefore, the germanene/MoSSe VHJs exhibit excellent stability and can be implemented experimentally. Furthermore, the binding energy E_b of the constructed heterojunction can be calculated by the following formula:

$$E_b = \frac{E_{\text{tot}} - E_{\text{Ge}} - E_{\text{MoSSe}}}{A}, \tag{1}$$

where E_{tot}, E_{Ge}, and E_{MoSSe} represent the total energies of germanene/MoSSe VHJs ($3 \times 3 \times 1$) supercell of germanene and ($\sqrt{13} \times \sqrt{13} \times 1$) supercell of Juans MoSSe, respectively. A stands for the area of the supercell of heterojunction. Then, the binding energies of Ge/SMoSe and Ge/SeMoS VHJs were calculated to be −5.93 and −6.23 meV/Å^2 (Table I), respectively, which indicates these configurations are energetically stable. It could be speculated that the different stability of the constructed heterojunctions is related with the different electronegativity of S and Se atoms. Thus, Ge/SeMoS heterojunction is more stable due to the S atom with large electronegativity is far from germanene. The Ge/SeMoS VHJ is more stable due to lower binding energy.

For a better understanding of the effect of monolayer on the heterojunction, Fig. 5 gives the band structures of ($3 \times 3 \times 1$)

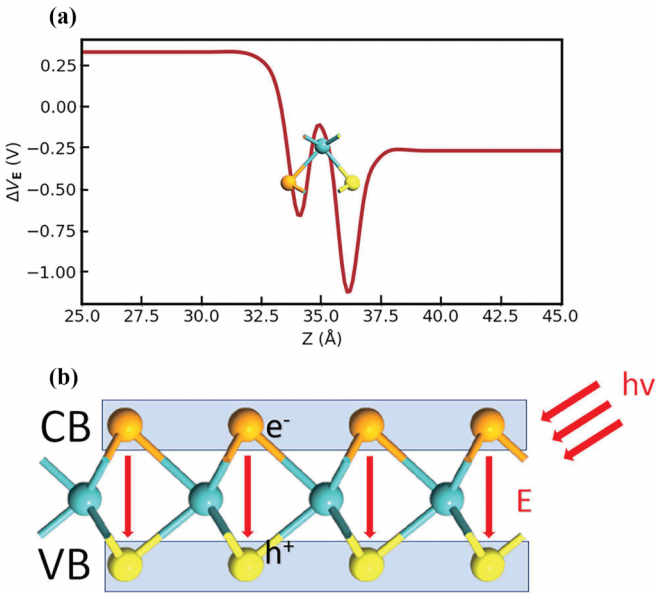

FIG. 3. (a) The electrostatic difference potential along z axis of monolayer MoSSe; (b) schematic diagram of photogenerated carriers in MoSSe and built-in electric field from Se to S.

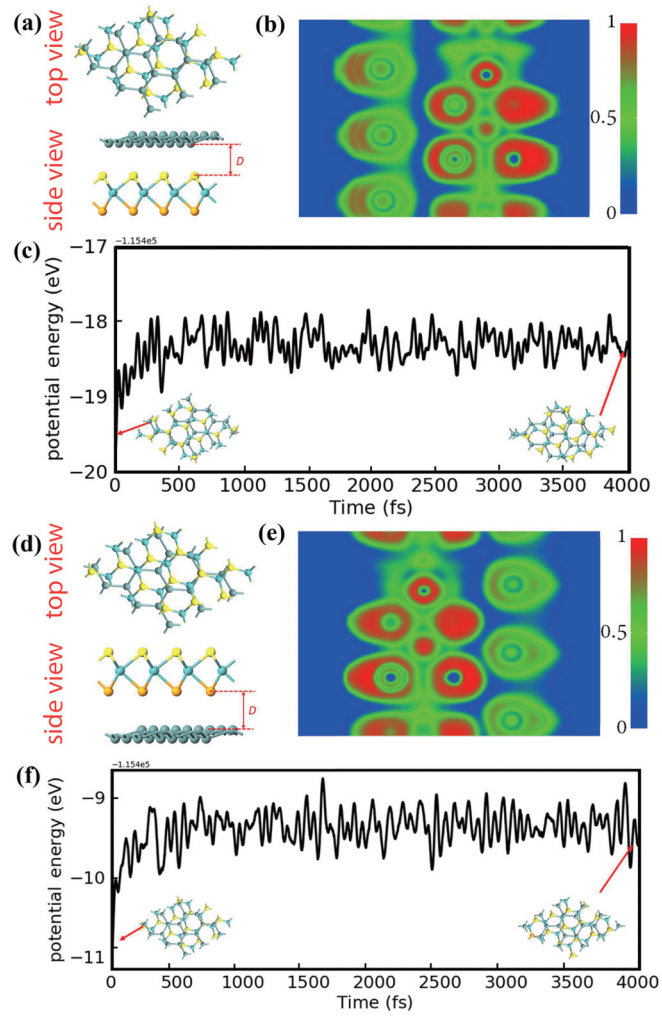

FIG. 4. Geometric structures of (a) Ge/SMoSe and (d) Ge/SeMoS VHJs. Electron location function of (b) Ge/SeMoS and (e) Ge/SMoSe VHJs. AIMD simulation for the change of potential energy of (c) Ge/SeMoS and (f) Ge/SMoSe VHJs as a function of heating time at room temperature (300 k). The insets represent snapshots of atoms structures of the germanene/MoSSe VHJs before and after heating of 4 ps.

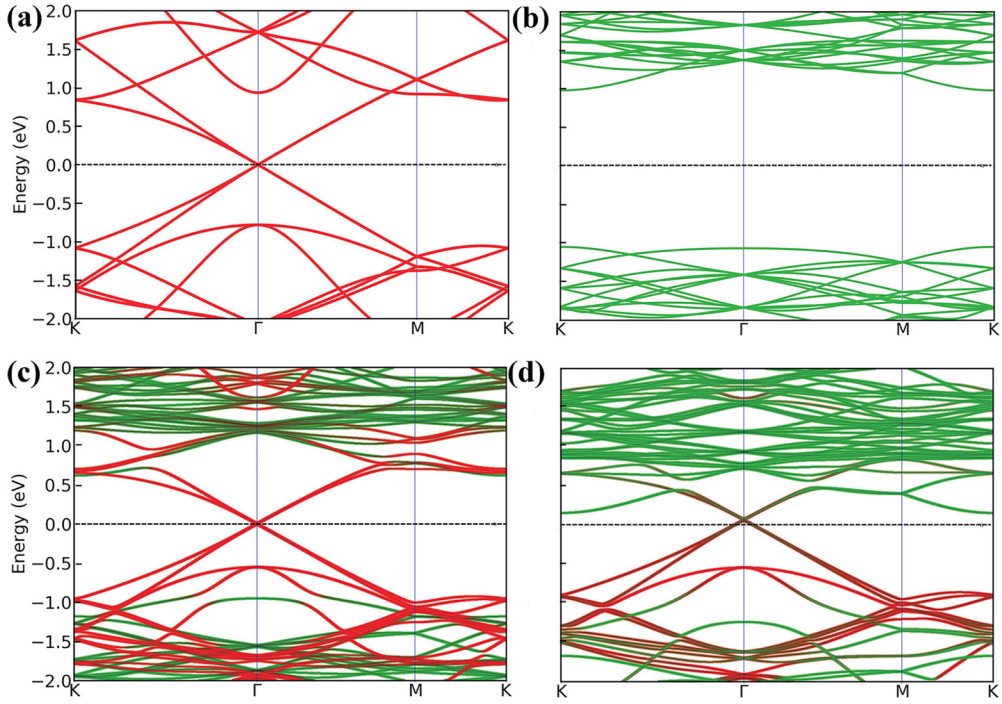

FIG. 5. Band structures of (a) $(3 \times 3 \times 1)$ germanene supercell and (b) $(\sqrt{13} \times \sqrt{13} \times 1)$ MoSSe supercell, projected band structures of (c) Ge/SeMoS and (d) Ge/SMoSe VHJs. Red and green lines represent the contributions of germanene and Janus MoSSe monolayers, respectively.

germanene supercell and $(\sqrt{13} \times \sqrt{13} \times 1)$ MoSSe supercell, and the projected band structures of germanene/MoSSe VHJ, respectively. In Fig. 5(a), the Dirac cone in the band structure locates at the Γ point, which is different from that of the germanene primitive unit cell, due to the folding effect. From Fig. 5(b), it can be seen that CBM and VBM of MoSSe supercell at K point are 0.98 eV and −1.05 eV, respectively, so Janus MoSSe supercell has a direct band gap of 2.03 eV, which is the same as that of MoSSe primitive unit cell. The Fermi level of MoSSe is closer to conduction band than the valence band, indicating that MoSSe is an n-type semiconductor. Furthermore, comparing with Figs. 5(a) and 5(b), the band structures of Ge/SeMoS [Fig. 5(c)] and Ge/SMoSe [Fig. 5(d)] are factually the combinations of band structures of the constituent monolayers, and the opened germanene band gap is 15.78 and 17.3 meV, respectively. The Dirac cone of germanene/MoSSe origins from germanene, whereas the n-type semiconductor characteristic of Janus MoSSe is still reflected in the heterojunction. Therefore, the electronic properties of germanene/MoSSe VHJs can be attributed to that of germanene and MoSSe monolayers because of the weak vdW interlayer interaction.

Here, it is noted that the band gap of germanene is opened after stacking the germanene and MoSSe. However, the band gap of freestanding germanene is zero at the K point ($\boldsymbol{k} = \frac{4\pi}{\sqrt{3}a}(\frac{1}{2}, \frac{1}{2\sqrt{3}})$, where a is lattice constant) in the Brillouin zone. With the tight-binding model, the low-energy effective Hamiltonian of germanene monolayer is [53]

$$H = \begin{pmatrix} \epsilon_A & \gamma_0 f(\boldsymbol{k}) \\ \gamma_0 f(\boldsymbol{k})^* & \epsilon_B \end{pmatrix}, \tag{2}$$

with

$$f(k_x, k_y) = \sum_{i=1}^{3} e^{i\boldsymbol{k}\cdot\boldsymbol{\delta}_i} = e^{iak_x/\sqrt{3}} + 2e^{-iak_x/2\sqrt{3}} cos\left(\frac{1}{2}ak_y\right), \tag{3}$$

where A and B are two nonequivalent germanium atoms in the unit cell and denoted as $\alpha = A$ or B, then $\epsilon_\alpha = \langle \Phi_\alpha | H | \Phi_\alpha \rangle$, $\Phi_\alpha = \frac{1}{\sqrt{N}} \sum_{\boldsymbol{R}_l^\alpha} e^{i\boldsymbol{k}\cdot\boldsymbol{R}_l^\alpha} \phi(\boldsymbol{r} - \boldsymbol{R}_l^\alpha)$, $\boldsymbol{R}_l^\alpha$, ϕ, and N denote the atom position vectors, normalized Bloch wave function, and the number of cells, respectively,$\gamma_0 = -\langle \Phi_A | H | \Phi_B \rangle$. For freestanding germanene, $\epsilon_A = \epsilon_B = \gamma$, we can obtain the eigenvalue as

$$E_k = \gamma \pm \gamma_0 |f(\boldsymbol{k})|. \tag{4}$$

Since $f(\boldsymbol{k}) = 0$, E_k near the K point can be written as

$$E_k = \gamma. \tag{5}$$

It means that the freestanding germanene is gapless. In the heterojunctions, however, due to the low-buckled structures of germanene, it leads to the inequality of ϵ_A and $\epsilon_B (\epsilon_A \neq \epsilon_B)$. Thus, the eigenvalue is written as

$$E_k = \tfrac{1}{2}(\epsilon_A + \epsilon_B \pm E_g), \tag{6}$$

where $E_g = |\epsilon_A - \epsilon_B|$. Then, there is a band gap at the K point. When germanene is close to the S or Se layer, it leads to a different value of E_g and thus a different band gap.

From the perspective of the application, carrier mobility is an important parameter for the design of devices. As is well known, the carrier mobility is dependent on the effective mass of carriers m^* and relaxation time τ, and presented as follows: $\mu = e\tau/m^*$, where e represent electron charge and τ

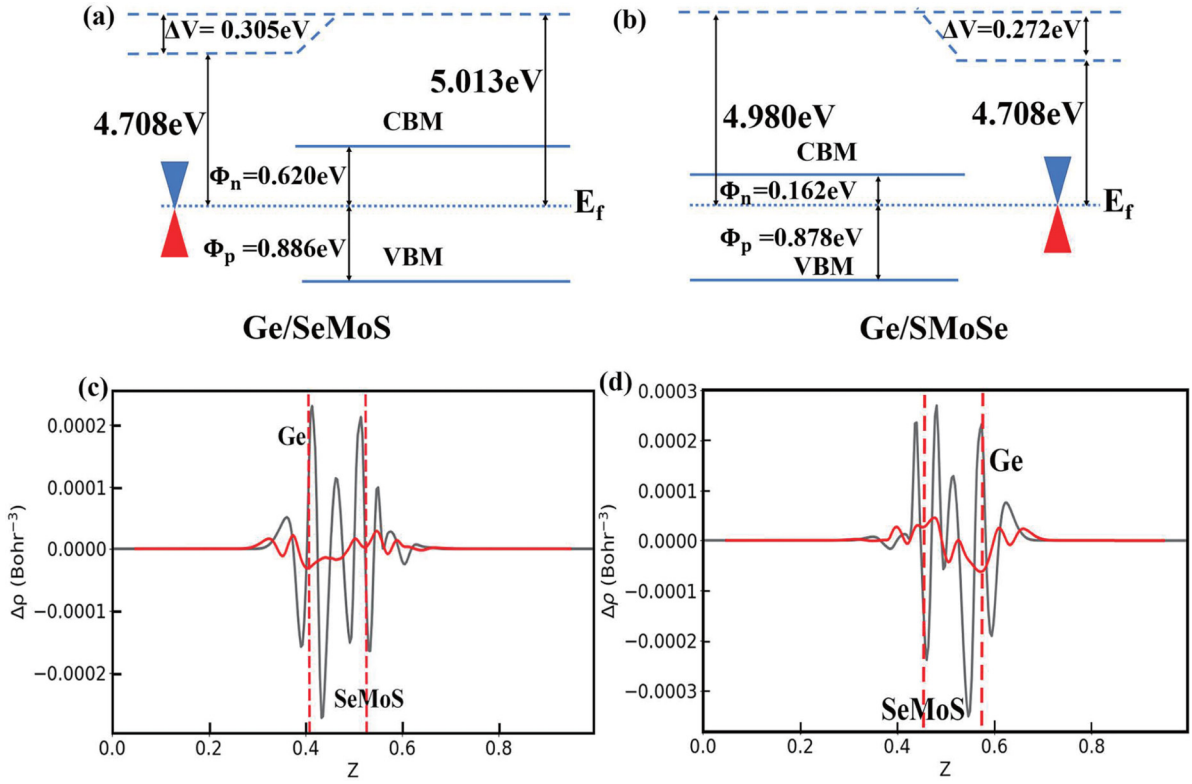

FIG. 6. Band alignment of germanene and Janus MoSSe monolayers of (a) Ge/SeMoS and (b) Ge/SMoSe VHJs. Electronic density different (black solid line) and its average value (red solid line) of (c) Ge/SeMoS and (d) Ge/SMoSe VHJs, the red dashed line indicates the centrally position of each layer.

relaxation time. The effective mass of the carrier is calculated using the following formula:

$$\frac{1}{m^*} = \frac{1}{\hbar}\frac{\partial^2 E(\boldsymbol{k})}{\partial \boldsymbol{k}^2}, \tag{7}$$

here, $\hbar$, $\boldsymbol{k}$, and $E(\boldsymbol{k})$ represent reduced Planck constant, wave vector, and the eigenvalues of energy band, respectively. From Eq. (7), the effective mass of holes and electrons can be obtained by parabolic fitting the VBM and CBM of heterojunction. For MoSSe monolayer, the average effective mass of carrier is 0.669 m_e (hole) and 0.532 m_e (electron), where m_e denotes electron mass, while for germanene monolayer, the average effective mass is massless. For Ge/SeMoS VHJ, the effective mass of carrier at Γ point was calculated to be 0.003 m_e (hole) and 0.005 m_e (electron), while for Ge/SMoSe VHJ the effective mass of carrier is 0.003 m_e (hole) and 0.003 m_e (electron). By comparing the band structure of freestanding germanene and the heterojunctions, it is found that the band structure of germanene in the heterojunction gets a little flat and has a band gap at Γ point, which leads to a small effective mass [54]. Considering the effect of electron-phonon coupling on relaxation time τ, the mobility can be obtained by solving the semiclassical Boltzmann transport equation (BTE) [55]. At 300 K and a carrier concentration of 3.01×10^{12} cm^{-2}, the mobility of carrier in the Ge/SeMoS VHJ are calculated to be 5.41×10^4 cm^2 V^{-1} s^{-1} (electron) and 1.29×10^5 cm^2 V^{-1} s^{-1} (hole), the calculations details see Supplemental Material [40]. Therefore, the constructed Ge/SeMoS VHJs are a favorable candidate for future high-speed devices.

In addition, the interfacial property of the heterojunction is also an essential factor in the design of the device, such as the contact type. For the germanene/MoSSe VHJs, two contact types, i.e., Schottky and Ohmic contacts, is possible within the interface of metal and semiconductors. From the band-edge values and Fermi level shown in Figs. 5(a)–5(c), it is easy to depict the band rearrangement before and after the Ge/SeMoS VHJ was constructed by germanene and Janus MoSSe monolayers. As shown in Fig. 6(a), after forming the heterojunction, the band gap of MoSSe is 1.506 eV and which is 0.524 eV smaller than that of freestanding MoSSe. Thus, it is determined that the interface of Ge/SeMoS VHJ is Schottky contact by comparing the band-edge positions of MoSSe layer relative to the Fermi level of heterojunction [56]. By the same argument, Fig. 6(b) shows the interface of Ge/SMoSe VHJ is also Schottky contact by the analysis of Figs. 5(a), 5(b), and 5(d). Furthermore, according to the metal induced gap state (MIGS) model and the charge neutrality level (CNL) model, the Schottky barrier heights are given by [57,58]

$$\begin{aligned} \Phi_n &= S(\Phi_m - \Phi_{\mathrm{CNL}}) + (\Phi_{\mathrm{CNL}} - \chi), \\ \Phi_p &= S(\Phi_m - \Phi_{\mathrm{CNL}}) + (\Phi_{\mathrm{CNL}} - \chi), \end{aligned} \tag{8}$$

where Φ_m is the work function of metal, E_g is the bandgap of semiconductor, S is the slope parameter, χ is the electron affinity and Φ_{CNL} is CNL. For an ideal metal-semiconductor interface, $S = 1$, whereas $0 \leqslant S < 1$ is corresponded to a non-ideal contact interface, in which $S = 0$ represents that SBH is not changed with variation of the work function of metal,

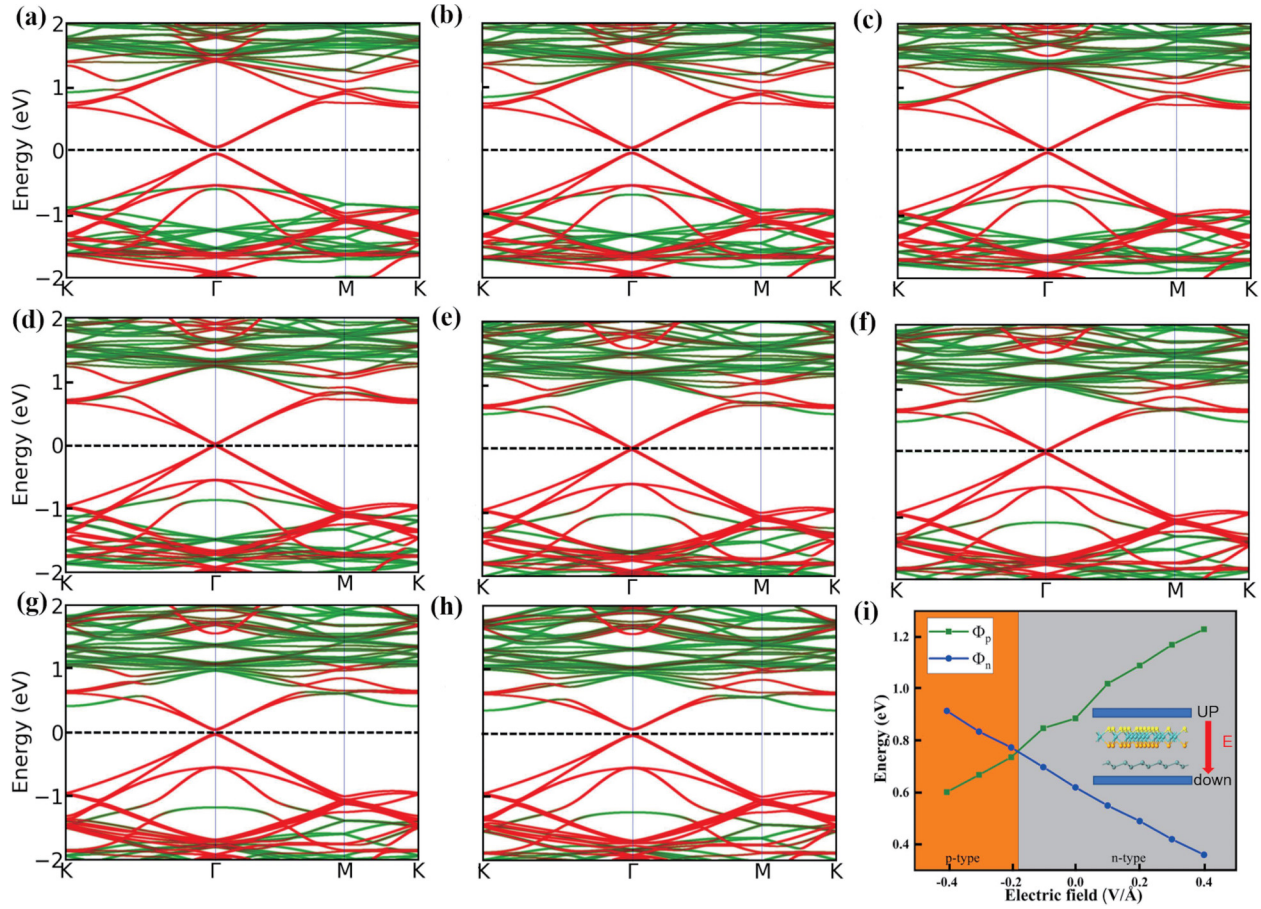

FIG. 7. Projected band structures of Ge/SeMoS VHJ under negative electric filed of (a) −0.4 V/Å, (b) −0.3 V/Å, (c) −0.2 V/Å, (d) −0.1 V/Å, and positive electric filed of (e) 0.1 V/Å, (f) 0.2 V/Å, (g) 0.3 V/Å, and (h) 0.4 V/Å. Red and green lines represent the contributions of germanene and Janus MoSSe layers, respectively. (i) The variation of SBH is as a function of the electric field, where the Φ_n and Φ_p under zero electric field come from FIG. 5(c). The insert displays the electric field applied on Ge/SeMoS VHJ which is introduced with the effective screening medium (ESM) medthod.

indicating a completely pinned interface at the CNL. In case of the germanene/MoSSe VHJs, as shown in Figs. 4(b) and 4(e), the interlayer interaction between germanene and MoSSe is the van der Waals interaction, thus the interlayer interface of Ge/MoSSe VHJs is ideal contact interface, that is $S = 1$ [59]. Therefore, Φ_n and Φ_p satisfy the Schottky-Mott rule, the Schottky barriers can be calculated by the following formulas [60,61]:

$$\Phi_n = E_c - E_f, \quad \Phi_p = E_f - E_v, \tag{9}$$

where E_f, E_c, E_v, Φ_n, and Φ_p represent the Fermi level, CBM, VBM, and the Schottky barrier height of n-type and p-type, respectively. The differences in Schottky barrier of the germanene/MoSSe VHJs ($\Delta\Phi = \Phi_p - \Phi_n$) are listed in Table I. It was found that all $\Delta\Phi$ is positive value (that is $\Phi_p > \Phi_n$), indicating the existence of p-type Schottky contact for both Ge/SeMoS and Ge/SMoSe VHJs. However, the charge densityd difference of the germanene/MoSSe VHJs was investigated to understand the charge redistribution and band alignment at the interface. We define the charge density difference $\Delta\rho(r)$ as

$$\Delta\rho(r) = \rho_{\text{heter}}(r) - \rho_{\text{Ge}}(r) - \rho_{\text{MoSSe}}(r), \tag{10}$$

where $\rho_{\text{heter}}(r)$, $\rho_{\text{Ge}}(r)$, and $\rho_{\text{MoSSe}}(r)$ represent the charge density of the heterojunction, freestanding germanene, and Janus MoSSe monolayer, respectively. As shown in Figs. 6(c) and 6(d), the average electronic density difference is a negative value, meaning the losing of electrons at the germanene layer, whereas the positive value means accumulation of electrons at the MoSSe layer. It proved that the electrons are transferred from the germanene to the MoSSe layer for both Ge/SeMoS and Ge/SMoSe.

Given the advantages of structure stability and experimental feasibility, the contact type and the Schottky barrier of the Ge/SeMoS VHJ were further investigated. Figures 7(a)–7(h) give the projected band structures of Ge/SeMoS VHJ for different external electric fields. It is easy to find that the Fermi level of Ge/SeMoS VHJ is gradually close to the conduction-band edge as the increasing of external electric fields from −0.4 to 0.4 V/Å. The Schottky barrier as a function of the external electric fields is presented in Fig. 7(i), which shows that Φ_n linearly decreases with increasing electric field, whereas Φ_p linearly increases with increasing electric field. In particular, Φ_n and Φ_p intersect at −0.185 V/Å, indicating the transform of Schottky barrier from p-type to n-type at this cross point. And for positive electric field, i.e., the intensities

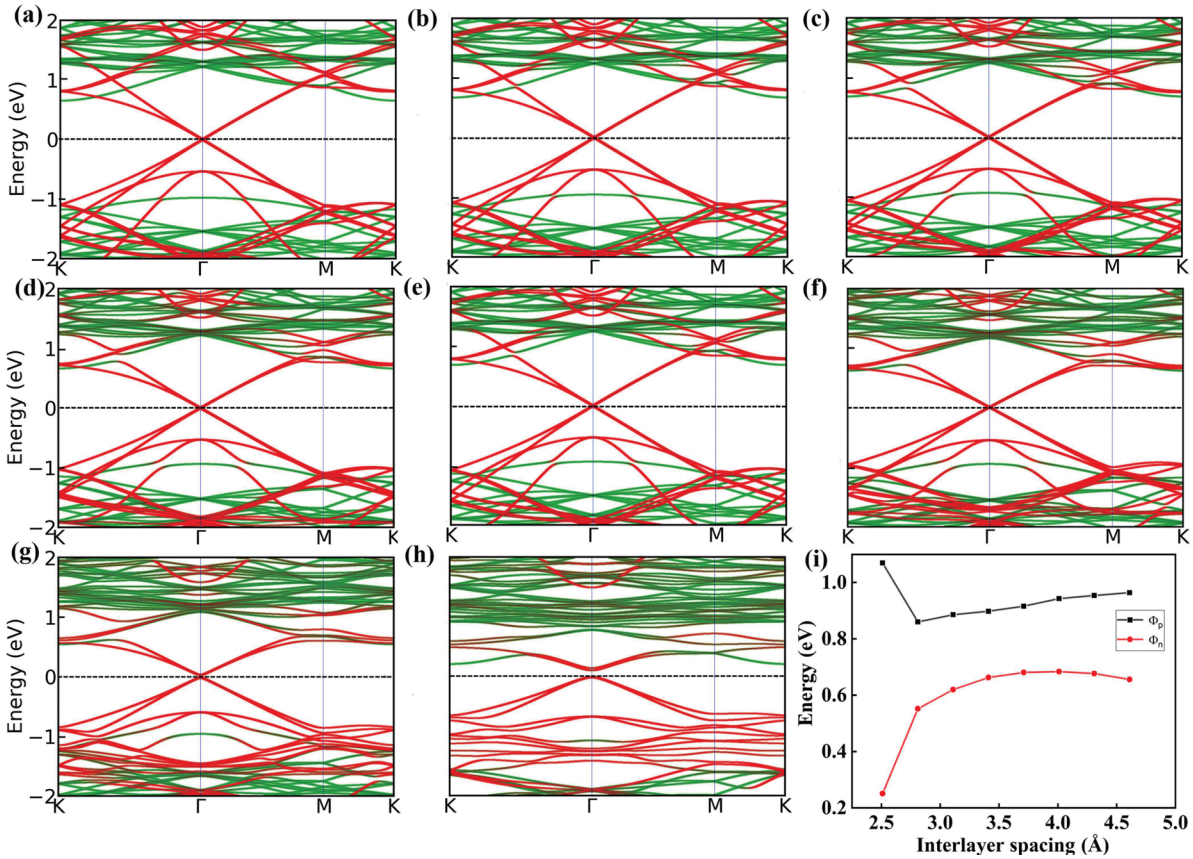

FIG. 8. Band structures of Ge/SeMoS VHJ with the interlayer distances of (a) 4.61 Å, (b) 4.31 Å, (c) 4.01 Å, (d) 3.71 Å, (d) 3.41 Å, (f) 3.11 Å, (g) 2.81 Å, and (h) 2.51 Å. (i) The n-type and p-type of SHB as function of interlayer distance

of the external electric field larger than zero, Φ_p is always larger than Φ_n, suggesting that the Ge/SeMoS VHJ always maintains to be n-type Schottky barrier. Furthermore, it can be inferred that Φ_n will decrease to zero with further increase of external electric field, which means that the contact type would become Ohmic contact. In other words, by introducing the external electric fields, the Schottky barrier of Ge/SeMoS VHJ can be switched from p-type to n-type, and even the contact type can be changed from Schottky contact to Ohmic contact.

In fact, the Schottky barrier of Ge/SeMoS VHJ dependent on the external electric field can be attributed to the electronic moving against the direction of electric field and the shift of Fermi energy levels. For the applied positive electric field the electrons are transferred to the S side of the Janus MoSSe monolayer, more electrons are concentrated in the MoSSe and lead to the Fermi energy level shifting upward, but the Fermi energy level shifts downward for the applied negative electric field. However, in the case of external electric field, Eq. (2) can be written as [53]

$$H = \begin{pmatrix} \gamma & \gamma_0 f(\boldsymbol{k}) \\ \gamma_0 f(\boldsymbol{k})^* & \gamma + eE_\perp \Delta \end{pmatrix}, \tag{11}$$

where $E_\perp$ is the electric field perpendicular to the interface and Δ denotes the bucking of germanene. Then the eigenvalue is

$$E_k = \gamma + \frac{eE_\perp \Delta}{2} \pm \sqrt{\gamma_0^2 f(\boldsymbol{k}) + \frac{1}{4}(eE_\perp \Delta)^2}. \tag{12}$$

Then, E_k at the K point can be approximated as

$$E_k = \gamma + \frac{eE_\perp \Delta}{2} \pm \left[\frac{E_\perp e\Delta}{2} + \frac{\gamma_0^2 f(\boldsymbol{k})}{E_\perp e\Delta} \right]. \tag{13}$$

Apparently, the band gap $E_g = E_\perp e\Delta \propto E_\perp$. Therefore, the band gap of Ge/SeMoS VHJ is increased with increases of the external electric field intensity.

In addition, the effect of interlayer coupling for Schottky barrier and contact type of Ge/SeMoS VHJ were investigated. The projected band structure and the Schottky barrier as a function of interlayer distance are depicted in Figs. 8(a)–8(g). Obviously, with the decrease of interlayer distance from 4.61 to 2.51 Å, the interlayer coupling becomes stronger, which leads to the gradual increase of the hybridization of bands structure of germanene and MoSSe monolayers. Particularly, it can be seen in Fig. 8(g) that the band structure of germanene experiences a heavy distortion so that its Dirac cone disappears for the narrow interlayer distance. This can be attributed to the strong interlayer coupling between germanene and MoSSe layers, and the interlayer interaction transforms from vdW to Coulomb type. In Fig. 8(h), apart from 2.51 Å, as the interlayer distance increases from 2.81 to 4.61Å, Φ_p of Ge/SeMoS VHJ always increases. However, Φ_n of Ge/SeMoS VHJ increases first and then decreases with increasing interlayer distances, and Φ_n is maximum at 4.01 Å. It can be found that with the increase of interlayer distance, the interlayer coupling becomes weaker, and Φ_p and Φ_n increase

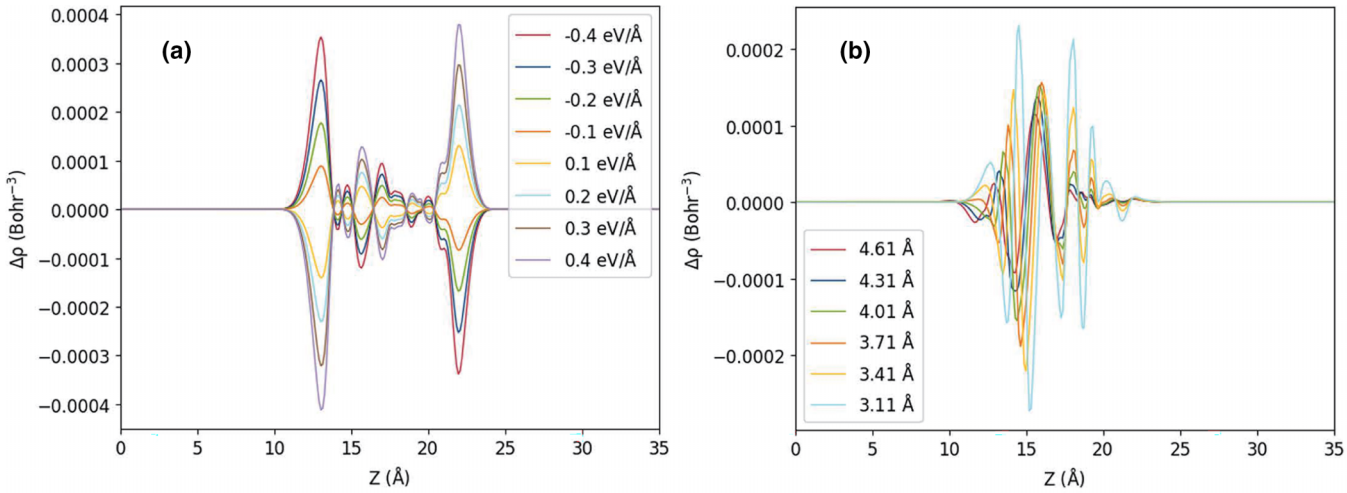

FIG. 9. Electron density difference of Ge/SeMoS VHJ for various of (a) electric fields and (b) interlayer spacing.

accordingly. However, with the further increase of distance, the n-type Schottky barrier of Ge/SeMoS VHJ shows a declining trend, that is, Φ_n decreases with the increase of layer distance, which is similar to the case of graphene-based vdW heterojunctions [29,62–64]. Thus, we can conclude that the interlayer distance engineering can effectively modulate the Schottky barrier of Ge/SeMoS VHJ, but the contact type of interface is unaltered.

To better understand the physical mechanism of Schottky barrier variation, the change of Fermi energy level is analyzed by calculating the electron density difference of the constructed Ge/SeMoS heterostructures under the modulation of electric field and interlayer coupling. Here, the electron density difference $\Delta\rho_E$ at an electric field is defined as

$$\Delta\rho_E = \rho_E - \rho_0, \tag{14}$$

where ρ_E and ρ_0 represent the electron density of the Ge/SeMoS VHJ under an electric field and zero electric field, respectively. Then, the $\Delta\rho_E$ of Ge/SeMoS VHJ corresponding to the electric fields in the range from −0.4 to 0.4 eV/Å are obtained and shown in Fig. 9(a). It can be found that the electron density of the MoSSe layer gradually become larger with increase of the external electric field, in other words, changing from losing electrons to gaining electrons. The increase of electron density leads to an upward shift of the Fermi energy level, so that Φ_p increases and Φ_n decreases, i.e., causing the transformation of Schottky barrier from the p-type to the n-type. However, based on Eq. (10), the electron density difference of Ge/SeMoS VHJ with different layer spacing is shown in Fig. 9(b). As decrease of the interlayer spacing, it can be found that the electrons of germanene layer are gradually close to MoSSe layer, and the electrons in MoSSe layer are redistributed and transferred from S-side to Se-side, which leads to the variation of Φ_n and Φ_p are almost synchronized, so the type of Schottky barrier is not changed. In addition, it should be pointed out that, for the heterostructure with an interlayer spacing of 2.81 Å, the electron density difference shown in Fig. S3(a) is significantly different from that in Fig. 9(b), and the electron location function [Fig. S3(b)] indicates that there are covalent bonds between Ge and MoSSe layers, which implies the forming of a non-van der Waals heterostructure [40].

Finally, the optical absorption behavior of Ge/SeMoS VHJ was studied. As well known, the optical absorption of material is dependent on the dielectric functions. According to Refs. [65,66], the susceptibility $\boldsymbol{\chi}(\omega)$ written as

$$\chi_{\alpha\beta}(\omega) = \frac{e^2}{\hbar m_e^2 V}\sum_{nm\boldsymbol{k}}\frac{f_{m\boldsymbol{k}} - f_{n\boldsymbol{k}}}{\omega_{nm}^2(\boldsymbol{k})[\omega_{nm}(\boldsymbol{k}) - \omega - i\Gamma/\hbar)]} \times p_{nm}^{\alpha}(\boldsymbol{k})p_{nm}^{\beta}(\boldsymbol{k}), \tag{15}$$

where $p_{nm}^{l}(\boldsymbol{k}) = \langle n\boldsymbol{k}|\,\hat{P}_l\,|m\boldsymbol{k}\rangle$, $\hat{P}_l$ is the lth ($l = \alpha, \beta$) component of the momentum operator, n and m are electronic state, m_e and e are the electron mass and the electron charge, respectively, V is the volume of lattice, Γ the energy broadening, $\hbar\omega_{nm} = E_n - E_m$, and $f_{n\boldsymbol{k}}$ is the Fermi function evaluated at the band energy $E_n(\boldsymbol{k})$. The dielectric function $\boldsymbol{\epsilon}_r$ is related to the $\boldsymbol{\chi}(\omega)$ and can be written as

$$\boldsymbol{\epsilon}_r(\omega) = 1 + \boldsymbol{\chi}(\omega) = \epsilon_1 + i\epsilon_2, \tag{16}$$

where ϵ_1 and ϵ_2 are the real and imaginary part of dielectric function, respectively. Then, the optical absorption coefficient can be calculated as follows:

$$\alpha(\omega) = \frac{\omega}{c}\sqrt{2\left[\sqrt{\epsilon_1^2(\omega) + \epsilon_2^2(\omega)} - \epsilon_1(\omega)\right]}, \tag{17}$$

here, ω and c are frequency and velocity of light, $\epsilon_1(\omega)$ and $\epsilon_2(\omega)$ are the real part and imaginary part of the dielectric function associated with the stored energy and the dissipation of energy within the medium, respectively [67]. The real and imaginary parts of the dielectric function and the optical absorption coefficient of Ge/SeMoS VHJ were calculated and shown in the Fig. 10. As an important index to evaluate the performance of material, it is clear from Fig. 10(a) that the static lattice dielectric constant $\epsilon_1(0)$ of germanene, Janus MoSSe, and Ge/SeMoS VHJ are 1.32, 1.44, and 2.55, respectively. Obviously, the static lattice dielectric constant of Ge/SeMoS VHJ is larger than that of monolayers. It illustrates that the energy storing capacity of the heterojunction is significantly enhanced compared with that of monolayers.

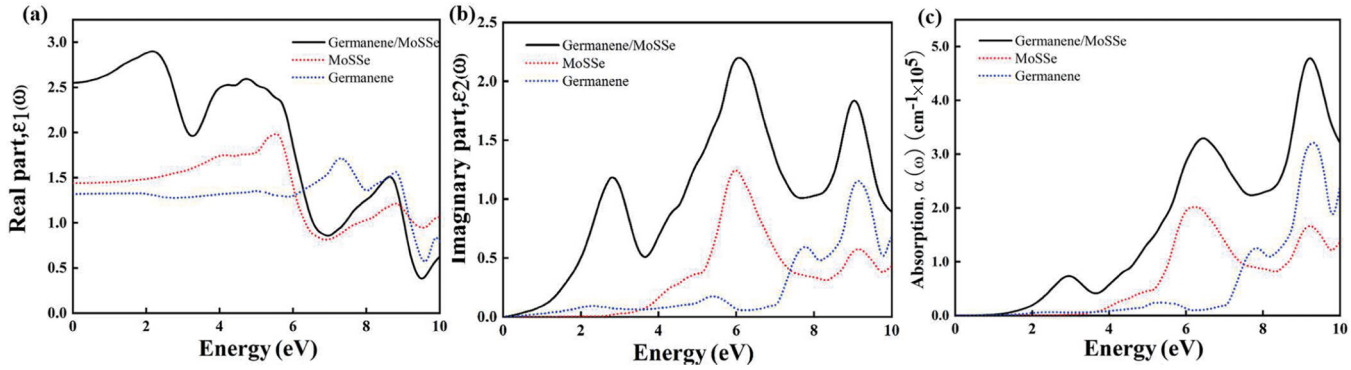

FIG. 10. (a) Real part and (b) imaginary part of dielectric function and (c) optical absorption spectrum of Ge/SeMoS VHJ, freestanding germanene, and Janus MoSSe monolayers.

From Fig. 10(b), it can be seen that the imaginary part $\epsilon_2(\omega)$ of the Ge/SeMoS VHJ is much larger than that of monolayers, indicating a significant energy dissipation of the heterojunction. As shown in Fig. 10(c), the germanene and Janus MoSSe monolayers have strong absorption in the ranges of photon energy of >7.02 eV and >4 eV, respectively. However, the Ge/SeMoS VHJ exhibits even stronger absorption in a wider range of photon energy. Such a phenomenon also arises in other heterostructures [62].

In addition, we can find from Fig. 10(c) that the Ge/SeMoS VHJ has an absorption peak near 3 eV, but there is no peak in the case of monolayer. It can be accounted by the susceptibility $\chi(\omega)$ of materials. From Eq. (15), for the monolayers, it could be speculated that the negligible absorption indicates the transition matrix element $p^l_{nm}(\boldsymbol{k})$ is zero, which inferred a forbidden transition near 3 eV. Inversely, for the Ge/SMoSe heterojunction, the electron transition is permissible. It suggest that Ge/SeMoS is a very promising optical material. Moreover, the exciton effect is an important factor affecting the optical 2D properties of the material [68,69], and will be further investigated in our work later.

IV. CONCLUSION

In summary, aside from the electric properties of germanene and Janus MoSSe monolayers, the electronic structure, stacking mode, mobility, and interface characteristics of germanene/MoSSe VHJs were investigated in depth by the first principles calculation. We found that the bandgap of germanene is opened and the carrier exhibit high mobility in the constructed heterostructures. And, under the modulation of external electric field, the contact types of Ge/SeMoS heterostructure undergo a transition from p-type Schottky barrier to n-type Schottky barrier, and even to Ohmic contacts. Moreover, the bandgap of the heterostructure increases with increasing the intensity of external electric field. However, for the modulation of interlayer coupling, although the interlayer distance can also change the Schottky barrier, the contact type at the interface remains unchanged. It suggests that electric field engineering is an effective strategy for regulating the Schottky barrier and the contact types of germanene/MoSSe VHJ. In addition, the calculation of absorption coefficient revealed that light absorption performance of Ge/SeMoS VHJ is greatly enhanced concerning that of the monolayers. Therefore, the excellent optoelectronic properties of the Ge/SeMoS VHJ demonstrate great application potential for high-performance optoelectronic devices.

ACKNOWLEDGMENTS

This work was supported by the National Natural Science Foundation of China (Grants No. 61675104, No. 21774067, No. 62075109, and No. 62135011). The work was also supported in part by the National Natural Science Foundation of China (Grants No. 61875250 and No. 61975189), the Zhejiang Provincial Natural Science Foundation of China (Grant No. LD21F050001) and the Key Research Project by Department of Water Resources of Zhejiang Province (Grant No. RA2101). The work was also supported in part by the Natural Science Fundation of Ningbo (Grant No. 2023J177).

[1] K. S. Novoselov, A. K. Geim, S. V. Morozov, D. Jiang, Y. Zhang, S. V. Dubonos, I. V. Grigorieva, and A. A. Firsov, Science **306**, 666 (2004).
[2] Y. W. Zhu, S. Murali, W. W. Cai, X. S. Li, J. W. Suk, J. R. Potts, and R. S. Ruoff, Adv. Mater. **22**, 3906 (2010).
[3] F. Bonaccorso, Z. Sun, T. Hasan, and A. C. Ferrari, Nat. Photon. **4**, 611 (2010).
[4] A. H. Castro Neto, F. Guinea, N. M. R. Peres, K. S. Novoselov, and A. K. Geim, Rev. Mod. Phys. **81**, 109 (2009).
[5] M. A. Rafiee, J. Rafiee, Z. Wang, H. H. Song, Z. Z. Yu, and N. Koratkar, ACS Nano **3**, 3884 (2009).
[6] U. K. Sur, Int. J. Electrochem. Sci. **2012**, 237689 (2012).
[7] Y. Sun, Q. Wu, and G. Shi, Energy Environ. Sci. **4**, 1113 (2011).
[8] L. Feng and Z. Liu, Nanomedicine **6**, 317 (2011).
[9] S. Manzeli, D. Ovchinnikov, D. Pasquier, O. V. Yazyev, and A. Kis, Nat. Rev. Mater. **2**, 17033 (2017).
[10] M. Naguib, V. N. Mochalin, M. W. Barsoum, and Y. Gogotsi, Adv. Mater. **26**, 992 (2014).
[11] S. Balendhran, S. Walia, H. Nili, S. Sriram, and M. Bhaskaran, Small **11**, 640 (2015).
[12] K. Watanabe, T. Taniguchi, and H. Kanda, Nat. Mater. **3**, 404 (2004).

[13] S. Cahangirov, M. Topsakal, E. Aktürk, H. Şahin, and S. Ciraci, Phys. Rev. Lett. **102**, 236804 (2009).

[14] A. Acun, L. Zhang, P. Bampoulis, M. Farmanbar, A. van Houselt *et al.*, J. Phys.: Condens. Matter **27**, 443002 (2015).

[15] E. Bianco, S. Butler, S. Jiang, O. D. Restrepo, W. Windl, and J. E. Goldberger, ACS Nano **7**, 4414 (2013).

[16] A.-Y. Lu, H. Zhu, J. Xiao, C.-P. Chuu, Y. Han, M.-H. Chiu, C.-C. Cheng, C.-W. Yang, K.-H. Wei, Y. Yang, Y. Wang, D. Sokaras, D. Nordlund, P. Yang, D. A. Muller, M.-Y. Chou, X. Zhang, and L.-J. Li, Nat. Nanotechnol. **12**, 744 (2017).

[17] C. Xia, W. Xiong, J. Du, T. Wang, Y. Peng, and J. Li, Phys. Rev. B **98**, 165424 (2018).

[18] A. C. Riis-Jensen, T. Deilmann, T. Olsen, and K. S. Thygesen, ACS Nano **13**, 13354 (2019).

[19] X. C. Ma, X. Wu, H. D. Wang, and Y. C. Wang, J. Mater. Chem. A **6**, 2295 (2018).

[20] W.-J. Yin, B. Wen, G.-Z. Nie, X.-L. Wei, and L.-M. Liu, J. Mater. Chem. C **6**, 1693 (2018).

[21] M. Idrees, H. U. Din, R. Ali, G. Rehman, T. Hussain, C. V. Nguyen, I. Ahmad, and B. Amin, Phys. Chem. Chem. Phys. **21**, 18612 (2019).

[22] Y. Y. Wang, Z. Y. Ni, Q. H. Liu, R. G. Quhe, J. X. Zheng, M. Ye, D. P. Yu, J. J. Shi, J. B. Yang, J. Li, and J. Lu, Adv. Funct. Mater. **25**, 68 (2015).

[23] A. K. Geim and I. V. Grigorieva, Nature (London) **499**, 419 (2013).

[24] H. Xu, J. Wu, Q. Feng, N. Mao, C. Wang, and J. Zhang, Small **10**, 2300 (2014).

[25] Y. X. Deng, Z. Luo, N. J. Conrad, H. Liu, Y. J. Gong, S. Najmaei, P. M. Ajayan, J. Lou, X. F. Xu, and P. D. Ye, ACS Nano **8**, 8292 (2014).

[26] A. Nourbakhsh, A. Zubair, M. S. Dresselhaus, and T. Palacios, Nano Lett. **16**, 1359 (2016).

[27] Q. Pang, H. Xin, D. l. Gao, J. Zhao, R. p. Chai, and Y. l. Song, Mater. Today Commun. **26**, 101845 (2021).

[28] X. Gao, Y. Shen, Y. Ma, S. Wu, and Z. Zhou, Phys. Status Solidi B **256**, 1800759 (2019).

[29] Y. Li, J. Wang, B. Zhou, F. Wang, Y. Miao, J. Wei, B. Zhang, and K. Zhang, Phys. Chem. Chem. Phys. **20**, 24109 (2018).

[30] N. Zhao and U. Schwingenschlögl, Nanoscale **12**, 11448 (2020).

[31] Q. Pang, H. Xin, R.-p. Chai, D.-l. Gao, J. Zhao, Y. Xie, and Y.-l. Song, Nanomaterials **12**, 3498 (2022).

[32] F. Li, W. Wei, P. Zhao, B. Huang, and Y. Dai, J. Phys. Chem. Lett. **8**, 5959 (2017).

[33] M. Brandbyge, J. L. Mozos, P. Ordejon, J. Taylor, and K. Stokbro, Phys. Rev. B **65**, 165401 (2002).

[34] Atomistix ToolKit version 2021, Quantumwise A/S, www.quantumwise.com.

[35] J. P. Perdew, K. Burke, and M. Ernzerhof, Phys. Rev. Lett. **77**, 3865 (1996).

[36] J. P. Perdew, K. Burke, and M. Ernzerhof, Phys. Rev. Lett. **80**, 891 (1998).

[37] S. Grimme, J. Antony, S. Ehrlich, and H. Krieg, J. Chem. Phys. **132**, 154104 (2010).

[38] J. Heyd, G. E. Scuseria, and M. Ernzerhof, J. Chem. Phys. **118**, 8207 (2003).

[39] M. J. van Setten, M. Giantomassi, E. Bousquet, M. J. Verstraete, D. R. Hamann, X. Gonze, and G.-M. Rignanese, Comput. Phys. Commun. **226**, 39 (2018).

[40] See Supplemental Material at http://link.aps.org/supplemental/10.1103/PhysRevB.108.125404 for the results of convergence tests, a schematic of the selected monolayer supercell, electron location function of heterojunction with 2.18 Å, and the details of mobility calculation based on electron-phonon coupling; see also Ref. [55]

[41] N. J. Roome and J. D. Carey, ACS Appl. Mater. Interfaces **6**, 7743 (2014).

[42] J. Zhang, S. Jia, I. Kholmanov, L. Dong, D. Er, W. Chen, H. Guo, Z. Jin, V. B. Shenoy, L.Shi, and J. Lou, ACS Nano **11**, 8192 (2017).

[43] J. Kang, L. J. Zhang, and S. H. Wei, J. Phys. Chem. Lett. **7**, 597 (2016).

[44] A. Splendiani, L. S. Y., B. Zhang, T. S. Li, J. Kim, C. Y. Chim, G. Galli, and F. Wang, Nano Lett. **10**, 1271 (2010).

[45] L. Jelver, P. M. Larsen, D. Stradi, K. Stokbro, and K. W. Jacobsen, Phys. Rev. B **96**, 085306 (2017).

[46] P. Lu, X. Wu, W. Guo, and X. C. Zeng, Phys. Chem. Chem. Phys. **14**, 13035 (2012).

[47] J.-A. Yan, S.-P. Gao, R. Stein, and G. Coard, Phys. Rev. B **91**, 245403 (2015).

[48] A. D. Becke and K. E. Edgecombe, J. Chem. Phys. **92**, 5397 (1990).

[49] K. Koumpouras and J. A. Larsson, J. Phys.: Condens. Matter **32**, 315502 (2020).

[50] C. Lei, Y. Ma, X. Xu, T. Zhang, B. Huang, and Y. Dai, J. Phys. Chem. C **123**, 23089 (2019).

[51] G. Li, L. Zhang, W. Xu, J. Pan, S. Song, Y. Zhang, H. Zhou, Y. Wang, L. Bao, Y.-Y. Zhang, S. Du, M. Ouyang, S. T. Pantelides, and H.-J. Gao, Adv. Mater. **30**, 1804650 (2018).

[52] X. Chen, Q. Yang, R. Meng, J. Jiang, Q. Liang, C. Tan, and X. Sun, J. Mater. Chem. C **4**, 5434 (2016).

[53] Z. Ni, Q. Liu, K. Tang, J. Zheng, J. Zhou, R. Qin, Z. Gao, D. Yu, and J. Lu, Nano Lett. **12**, 113 (2012).

[54] C. Kittel and P. McEuen, *Introduction to Solid State Physics* (John Wiley & Sons, New York, NY, 2018).

[55] T. Gunst, T. Markussen, K. Stokbro, and M. Brandbyge, Phys. Rev. B **93**, 035414 (2016).

[56] J. Li, W. Liu, W. Zhou, J. Yang, H. Qu, Y. Hu, and S. Zhang, Phys. Rev. Appl. **17**, 054009 (2022).

[57] A. M. Cowley and S. M. Sze, J. Appl. Phys. **36**, 3212 (1965).

[58] T. Nakayama, Y. Kangawa, and K. Shiraishi, *Atomic Structures and Electronic Properties of Semiconductor Interfaces* (Elsevier, New York, NY, 2011).

[59] X. Liu, M. S. Choi, E. Hwang, W. J. Yoo, and J. Sun, Adv. Mater. **34**, 2108425 (2021).

[60] P. Zhao, H. Jin, X. S. Lv, B. B. Huang, Y. D. Ma, and Y. Dai, Phys. Chem. Chem. Phys. **20**, 16551 (2018).

[61] J. Bardeen, Phys. Rev. **71**, 717 (1947).

[62] H. T. T. Nguyen, M. M. Obeid, A. Bafekry, M. Idrees, T. V. Vu, H. V. Phuc, N. N. Hieu, L. T. Hoa, B. Amin, and C. V. Nguyen, Phys. Rev. B **102**, 075414 (2020).

[63] C. V. Nguyen, M. Idrees, H. V.Phuc, N. N.Hieu, N. T. T. Binh, B. Amin, and T. V. Vu, Phys. Rev. B **101**, 235419 (2020).
[64] C. V. Nguyen, Phys. Rev. B **103**, 115429 (2021).
[65] J. E. Sipe and E. Ghahramani, Phys. Rev. B **48**, 11705 (1993).
[66] W. A. Harrison, *Solid State Theory* (Tata McGraw Hill Publishing, New York, NY, 1970).
[67] G. R. Berdiyorov, A. Kachmar, F. El-Mellouhi, M. A. Carignano, and M. E. Madjet, J. Phys. Chem. C **120**, 16259 (2016).
[68] G.-s. Shi and E. Kioupakis, Nano Lett. **15**, 6926 (2015).
[69] A. Ramasubramaniam, Phys. Rev. B **86**, 115409 (2012).